International Journal of
Science, Architecture, Technology and Environment

Adaptive Gain Sliding Mode Control for Quadrotor UAV Trajectory Tracking Under Full Nonlinear Dynamics

Khuat Quang Tien[1*]

[1]*Faculty of Fundamental Technical, Air Defence-Air Force Academy, Ha Noi, Viet Nam*

[*]*Corresponding author email: quangtienmta@gmail.com*

DOI: https://doi.org/10.63680/ijsate062655.59

Abstract

This paper presents an Improved Adaptive Sliding Mode Control (IASMC) synthesis method for quadrotor UAV systems based on the full nonlinear dynamics model derived from the Newton–Euler formulation. A quadrotor is characterized by strong nonlinearities, six degrees of freedom, and tight coupling among axes, which makes trajectory–tracking control challenging under disturbances and parameter uncertainties. The proposed method extends the classical sliding mode controller by integrating a channel–wise adaptive law, allowing dynamic adjustment of the control gain according to the error magnitude, thereby reducing chattering while maintaining Lyapunov stability. The complete quadrotor model is analyzed, sliding surfaces and equivalent control laws are clearly constructed, followed by integrating an adaptive component with a saturation function to enhance smoothness and tracking performance. The analysis results demonstrate that the IASMC guarantees global stability, improves accuracy and disturbance rejection capability, and is suitable for practical implementation on UAVs with actuator power limits and motor delays.

Keywords: Quadrotor UAV; Sliding Mode Control; Adaptive Control; Newton–Euler; Nonlinear System; Lyapunov; Chattering.

1. Introduction

In recent years, quadrotor unmanned aerial vehicles (UAVs) have become one of the most widely used aerial platforms in both civilian and military applications such as surveillance, search–and–rescue, smart transportation, and sensor data acquisition. The outstanding advantages of quadrotors include simple mechanical structure, good maneuverability, and low manufacturing cost. However, controlling a quadrotor remains highly challenging due to its strongly nonlinear nature, tight cross–coupling between axes, and the presence of external disturbances as well as parameter uncertainties.

Many control methods have been developed, such as extended PID, feedback linearization, model predictive control, optimal control, or adaptive control. However, these methods still exhibit limitations under fast–changing conditions, especially when the quadrotor operates in environments with wind and aerodynamic disturbances. Sliding Mode Control (SMC) is well known for its high robustness and strong disturbance rejection capability, but it suffers from the chattering phenomenon—high–frequency control oscillations that affect system stability and motor lifespan.

To overcome this limitation, the paper proposes an IASMC, in which the control gain is automatically

adjusted according to the system error through an adaptive learning rule. This approach preserves the inherent robustness of SMC while significantly reducing chattering thanks to the use of a saturation function combined with a dynamic learning mechanism.

Before presenting the proposed method, the full nonlinear dynamics model of the quadrotor is derived using the Newton–Euler formulation. Sliding surfaces, equivalent control laws, and the adaptive law are then constructed. Finally, Lyapunov–based stability proof is provided to guarantee global stability of the closed–loop system. The IASMC method shows high potential for real UAV control thanks to its simplicity, efficiency, and ease of implementation.

2. Algorithm Synthesis

To accurately estimate the Roll (ϕ), Pitch (θ), and Yaw (ψ) angles in a 3DOF system, the Extended Kalman Filter (EKF) is constructed based on the nonlinear Euler ZYX kinematic model and inertial sensor data. The algorithm consists of two main parts: the state prediction model and the measurement update model.

A quadrotor aircraft is a nonlinear multivariable control system with six degrees of freedom, including three translational motions and three rotational motions.

Consider the inertial coordinate system $O_E(x_E, y_E, z_E)$ and the body–fixed coordinate system $O_B(x_B, y_B, z_B)$. The position and attitude vectors of the UAV are defined as:

$$\boldsymbol{r} = \begin{bmatrix} x \\ y \\ z \end{bmatrix}, \ \boldsymbol{\eta} = \begin{bmatrix} \phi \\ \theta \\ \psi \end{bmatrix} \tag{1}$$

With:

x, y, z : position of the UAV center of mass in the inertial frame (m);

ϕ, θ, ψ : roll, pitch, and yaw angles (deg);

The relationship between the linear velocity in the inertial frame and in the body frame:

$$\boldsymbol{r} = \boldsymbol{R}(\phi, \theta, \psi)\mathbf{v} \tag{2}$$

Where $\mathbf{v} = \begin{bmatrix} u & v & w \end{bmatrix}^T$ [m/s] is the velocity vector in the body frame.

The rotation matrix $\boldsymbol{R}$ is given by:

$$\boldsymbol{R} = (\phi, \theta, \psi) = \begin{bmatrix} c_\theta c_\psi & s_\phi s_\theta c_\psi - c_\phi s_\psi & c_\phi s_\theta c_\psi + s_\phi s_\psi \\ c_\theta s_\psi & s_\phi s_\theta s_\psi + c_\phi c_\psi & c_\phi s_\theta s_\psi - s_\phi c_\psi \\ -s_\theta & s_\phi c_\theta & c_\phi c_\theta \end{bmatrix} \tag{3}$$

With $s(\cdot)$ and $c(\cdot)$ denoting sine and cosine, respectively.

The Newton–Euler equations describe the overall kinematics and dynamics of the UAV and consist of two parts:

- Translational equations:

$$m\dot{\mathbf{v}} = \mathbf{F}_B - mg\boldsymbol{R}^T e_3 \tag{4}$$

Where:

m : UAV mass (kg);

$\mathbf{F}_B = \begin{bmatrix} 0 & 0 & U_1 \end{bmatrix}^T$: total force generated by four motors (N);

$e_3 = \begin{bmatrix} 0 & 0 & 1 \end{bmatrix}^T$;

$g = 9.81(m/s^2)$.

Expanding the translational equations on each axis:

$$\ddot{x} = \frac{U_1}{m}\left(\cos\phi \sin\theta \cos\psi + \sin\phi \sin\psi\right) \tag{5}$$

$$\ddot{y} = \frac{U_1}{m}\left(\cos\phi\sin\theta\cos\psi - \sin\phi\cos\psi\right) \quad (6)$$

$$\ddot{z} = \frac{U_1}{m}\cos\phi\cos\theta - g \quad (7)$$

- Rotational equations:

$$\boldsymbol{J}\dot{\boldsymbol{\omega}} + \boldsymbol{\omega}\times(\mathbf{J}\boldsymbol{\omega}) = \mathbf{M} \quad (8)$$

Where:

$\boldsymbol{\omega} = \begin{bmatrix} p & q & r \end{bmatrix}^T$ (deg/s);

p, q, r - angular rates about body axes x_B, y_B, z_B.

$\boldsymbol{J} = diag(J_x, J_y, J_z)$ (kg.m²);

$\mathbf{M} = \begin{bmatrix} U_2 & U_3 & U_3 \end{bmatrix}^T$ (N.m).

Specific rotational equations:

$$\dot{p} = \frac{U_2 + (J_y - J_z)qr}{J_x} \quad (9)$$

$$\dot{q} = \frac{U_3 + (J_z - J_x)qr}{J_y} \quad (10)$$

$$\dot{r} = \frac{U_4 + (J_x - J_y)pq}{J_z} \quad (11)$$

Forces and torques generated by rotor speeds ω_i (deg/s):

$$U_1 = b(\omega_1^2 + \omega_2^2 + \omega_3^2 + \omega_4^2) \quad (12)$$

$$U_2 = bl(\omega_2^2 - \omega_4^2) \quad (13)$$

$$U_3 = bl(\omega_3^2 - \omega_1^2) \quad (14)$$

$$U_4 = d(\omega_1^2 - \omega_2^2 + \omega_3^2 - \omega_4^2) \quad (15)$$

Where:

U_1: total lift (N);

U_2, U_3, U_4: roll, pitch, yaw torques (N·m);

b: thrust coefficient (N·s²/deg²);

d: drag coefficient (N·m·s²/deg²);

l: arm length (m).

Relationship between angular velocity and Euler angle rates:

$$\boldsymbol{\omega} = T(\phi,\theta)\begin{bmatrix}\dot{\phi}\\ \dot{\theta}\\ \dot{\psi}\end{bmatrix} = \begin{bmatrix}1 & 0 & -\sin\theta\\ 0 & \cos\phi & \cos\theta\sin\phi\\ 0 & -\sin\phi & \cos\theta\cos\phi\end{bmatrix}\begin{bmatrix}\dot{\phi}\\ \dot{\theta}\\ \dot{\psi}\end{bmatrix} \quad (16)$$

Combining (5)–(11), the full dynamic system is written as:

$$\dot{\boldsymbol{x}} = f(\boldsymbol{x}) + G(\boldsymbol{x})\boldsymbol{U} \quad (17)$$

Where $f(x)$ is contains nonlinear components due to rotational dynamics and gravity; $G(x)$ describes how control inputs U_i affect the motion.

$$\boldsymbol{x} = \begin{bmatrix} x, y, z, \phi, \theta, \psi, \dot{x}, \dot{y}, \dot{z}, p, q, r \end{bmatrix}^T \quad (18)$$

$$\boldsymbol{U} = \begin{bmatrix} U_1, U_2, U_3, U_4 \end{bmatrix}^T \quad (19)$$

Sliding surface and control error design. The error between actual and desired states is:

$$e_i = x_{i,d} - x_i, \quad \dot{e}_i = \dot{x}_{i,d} - \dot{x}_i \quad (20)$$

Where $x_{i,d}$ is the desired value.

Sliding surface:

$$s_i = \dot{e}_i + \lambda_i e_i, \quad \lambda_i > 0 \tag{21}$$

λ_i is the coefficient that defines the convergence rate of the error.

With $i \in \{x, y, z, \phi, \theta, \psi\}$.

General vector form:

$$\boldsymbol{s} = \boldsymbol{e} + \Lambda \boldsymbol{e}, \quad \Lambda = diag(\lambda_1, ..., \lambda_6) \tag{22}$$

From (5)–(7) and (9)–(11), the derivatives of the sliding surfaces are obtained:

$$\dot{s}_x = \ddot{x}_d - \frac{U_1}{m}\left(\cos\phi \sin\theta \cos\psi + \sin\phi \sin\psi\right) + \lambda_x(\dot{x}_d - \dot{x}) \tag{23}$$

$$\dot{s}_y = \ddot{y}_d - \frac{U_1}{m}\left(\cos\phi \sin\theta \cos\psi - \sin\phi \cos\psi\right) + \lambda_y(\dot{y}_d - \dot{y}) \tag{24}$$

$$\dot{s}_z = \ddot{z}_d - \left(\frac{U_1}{m}\cos\phi \cos\theta - g\right) + \lambda_z(\dot{z}_d - \dot{z}) \tag{25}$$

And for rotational angles:

$$\dot{s}_\phi = \ddot{\phi}_d - \frac{U_2 + (J_y - J_z)qr}{J_x} + \lambda_\phi(\dot{\phi}_d - \dot{\phi}) \tag{26}$$

$$\dot{s}_\theta = \ddot{\theta}_d - \frac{U_3 + (J_z - J_x)qr}{J_y} + \lambda_\theta(\dot{\theta}_d - \dot{\theta}) \tag{27}$$

$$\dot{s}_\psi = \ddot{\psi}_d - \frac{U_4 + (J_x - J_y)pq}{J_z} + \lambda_\psi(\dot{\psi}_d - \dot{\psi}) \tag{28}$$

Equivalent control law. On the sliding surface ($\dot{s} = 0$), the equivalent control inputs are:

$$U_{1,eq} = \frac{m(\ddot{z}_d + g - \lambda_z(\dot{z}_d - \dot{z}))}{\cos\phi \cos\theta} \tag{29}$$

$$U_{2,eq} = J_x(\ddot{\phi}_d + \lambda_\phi \dot{e}_\phi) + (J_y - J_z)qr \tag{30}$$

$$U_{3,eq} = J_y(\ddot{\theta}_d + \lambda_\phi \dot{e}_\theta) + (J_z - J_x)qr \tag{31}$$

$$U_{4,eq} = J_z(\ddot{\psi}_d + \lambda_\psi \dot{e}_\psi) + (J_x - J_y)pq \tag{32}$$

Improved Adaptive Sliding Mode Control Law. Combining $U_{i,eq}$ from (29)–(32) with the sliding–mode compensation term that uses a saturation function and channel–wise adaptive parameters, the improved adaptive sliding mode control law for each channel $i \in \{x, y, z, \phi, \theta, \psi\}$:

$$U_i(t) = U_{i,eq}(t) - k_i(t)\, sat\left(\frac{s_i(t)}{\varepsilon_i}\right) \tag{33}$$

Where U_x, U_y, U_z are correspond to U_1, and U_ϕ, U_θ, U_ψ correspond to U_2, U_3, U_4.

With $\varepsilon_i > 0$ is the boundary layer thickness, and: $sat(x) = \begin{cases} \text{sgn}(x), & |x| > 1 \\ x, & |x| \le 1 \end{cases}$.

To automatically adjust the control intensity according to the error magnitude and reduce chattering while maintaining stability, the adaptive updating law for $k_i(t)$ is designed as:

$$\dot{k}_i = \gamma_i |s_i| - \rho_i k_i, \quad \gamma_i > 0, \rho_i \ge 0 \tag{34}$$

Where:

k_i : adaptive sliding–mode control gain;

$\gamma_i > 0$: learning rate determining the adaptation speed;

$\rho_i \geq 0$: decay coefficient.

After computing U_1, U_2, U_3, U_4 they must be mapped to rotor squared speeds ω_i^2. Define: $\mathbf{\Omega} = \begin{bmatrix} \omega_1^2 & \omega_2^2 & \omega_3^2 & \omega_4^2 \end{bmatrix}^T$.

The allocation matrix $\boldsymbol{A}$:

$$\begin{bmatrix} U_1 \\ U_2 \\ U_3 \\ U_4 \end{bmatrix} = \begin{bmatrix} b & b & b & b \\ 0 & bl & 0 & -bl \\ -bl & 0 & bl & 0 \\ d & -d & d & -d \end{bmatrix} \begin{bmatrix} \omega_1^2 \\ \omega_2^2 \\ \omega_3^2 \\ \omega_4^2 \end{bmatrix} \tag{35}$$

Lyapunov Stability Proof. Choose the Lyapunov function:

$$V = \frac{1}{2}\sum_i s_i^2 + \frac{1}{2\gamma_i}\sum_i \left(k_i - k_i^*\right)^2 \tag{36}$$

Derivative:

$$\dot{V} = \sum_i s_i \dot{s}_i + \frac{1}{\gamma_i}\sum_i \left(k_i - k_i^*\right)\dot{k}_i \tag{37}$$

Substituting (23)–(25) into (34), and after rearrangement:

$$\dot{V} \leq -\sum_i b_i k_i s_i sat\left(\frac{s_i}{\varepsilon_i}\right) - \sum_i \rho_i \frac{\left(k_i - k_i^*\right)^2}{\gamma_i} \leq 0 \tag{38}$$

Based on the dynamic model, sliding surface design, adaptive control law, control allocation strategy, and Lyapunov stability analysis presented above, the overall functional structure of the proposed adaptive gain sliding mode controller can be summarized as shown in Figure 1.

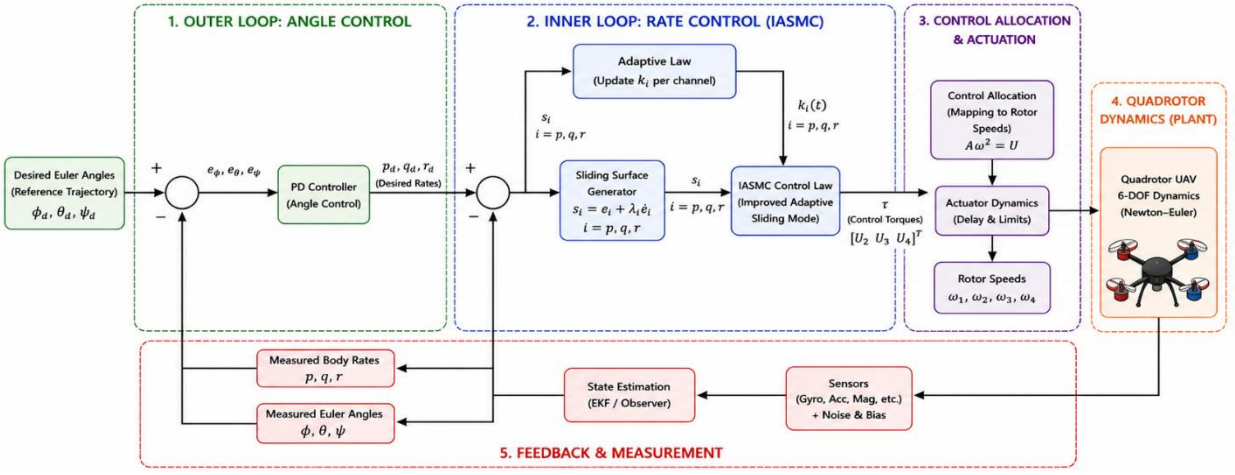

Figure 1. Functional Block Diagram of the Proposed Adaptive Gain Sliding Mode Controller for Quadrotor UAV

The above algorithm extends the classical sliding mode control method by incorporating a real–time adaptive law to adjust the control gain according to the error magnitude, enabling:

- Significant chattering reduction;
- Improved trajectory–tracking capability under disturbances;
- Preservation of global stability due to Lyapunov proof.

The improved adaptive sliding mode controller can be easily implemented in UAVs with actuator power limits and motor delays, and can be extended to other multi–DOF nonlinear systems.

3. Simulation and Evaluation

To verify the correctness and effectiveness of the designed EKF algorithm, simulations were carried out with 3DOF motion trajectory scenarios. The true angle signals (truth) were generated by combining multiple harmonic oscillations to reflect the complex motion characteristics of real-world objects. The sensor measurement data were simulated with full representative error factors such as Gaussian noise, constant bias error, and random bias drift modeled as random walk. At the same time, accelerometer and magnetometer measurements were simulated as Euler angles with Gaussian noise, serving as measurement sources for EKF updates. The simulation was conducted over sufficiently long durations to clearly show both the cumulative effects of sensor errors and the correction capability of the EKF. The performance evaluation criteria include Root Mean Square Error (RMSE), Mean Absolute Error (MAE), mean bias and Standard Deviation (STD), which were calculated to compare the "gyro-only" method with the EKF.

To verify the effectiveness of the proposed IASMC, this section performs a full dynamic simulation of the quadrotor system based on the six-degree-of-freedom Newton–Euler model. A two–loop control algorithm (outer–loop and inner–loop) is implemented to track time–varying Euler–angle trajectories, which require high adaptability and robustness against disturbances and model uncertainties. In addition, the adaptive algorithm is directly integrated into the angular–rate control channel to automatically adjust the sliding gain $k_i(t)$, thereby improving tracking performance and significantly reducing chattering compared with classical sliding mode control.

Simulations are conducted under various measurement noise conditions and random disturbance torques acting on the system to evaluate controller robustness. The results are presented as time responses of several important quantities, including actual and desired Euler angles and angular rates, tracking errors, sliding surfaces, control torques, and especially the evolution of the adaptive parameter $k_i(t)$. These results provide a comprehensive assessment of the stability, tracking quality, and robustness of the IASMC controller.

The IASMC algorithm is simulated using the following parameter set:

- Simulation time:12(s);
- Sampling step: 0.005(s);
- Moments of inertia: $I_{xx} = 0.008(kg.m^2)$, $I_{yy} = 0.008(kg.m^2)$, $I_{zz} = 0.014(kg.m^2)$;
- Gyroscope measurement noise: $\sigma_{sens} = [0.001, 0.001, 0.002](rad/s)$;
- External disturbance torques: $\sigma_{dist} = [0.01, 0.01, 0.02](Nm)$;
- Control torque limits: $\tau_{\max} = [0.25, 0.25, 0.40](Nm)$'
- Actuator delay: $\tau_{delay} = 0.008(s)$;
- Desired trajectory:

+ Roll angle: $\phi_d(t) = 12^0 \sin(0.6t)$;
+ Pitch angle: $10^0 \sin(0.8t + 0.25)$;
+ Yaw angle: $\psi_d(t) = 30^0 \sin(0.35t - 0.4)$;

- Outer-loop PD controller:

+ Proportional gains: $K_p = [6, 6, 8]$;
+ Derivative gains: $K_d = [2, 2, 2.5]$;
+ Set–point rate limit: $|\omega_d|_{\max} = 200(\deg/s)$;

- Inner-loop Adaptive Sliding Mode (ASMC):

+ Sliding surface coefficients: $\lambda = [8,8,10](1/s)$;

+ Saturation boundary layer: $\phi_{sat} = [0.03, 0.03, 0.05](rad/s)$;

+ Learning rates: $\gamma = [4,4,6]$

+ Decay coefficients: $\rho = [1,1,1]$

+ Maximum desired adaptive gains: $k^{\backslash *} = [2,2,3]$;

+ Initial gains: $k_i(0) = [0.2, 0.2, 0.3]$.

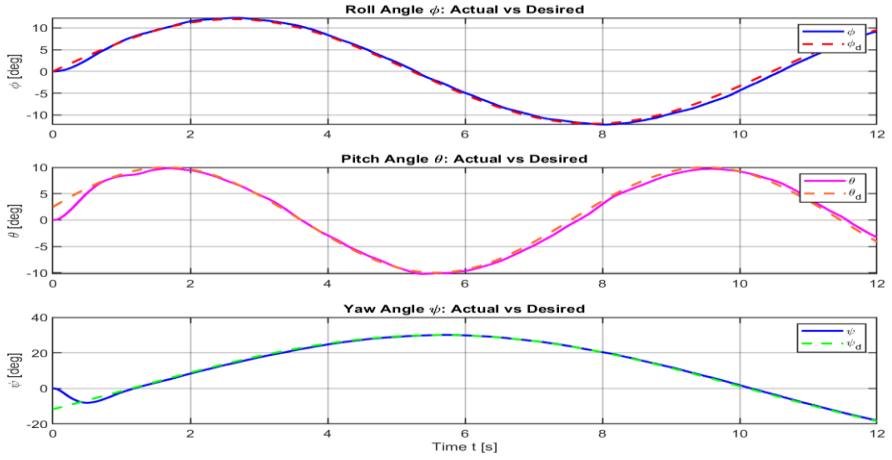

Figure 2. Euler Angle Tracking Performance

Figure 2 illustrates the Euler–angle tracking capability of the adaptive sliding mode controller. It can be observed that all three angles, roll (ϕ), pitch (θ), and yaw (ψ), closely follow the reference signals, even when the input trajectories are sinusoidal with different amplitudes and frequencies. Notably, the transient response duration of all three axes is short, approximately 0.5 to 1.2 seconds depending on the axis. The difference between actual and desired trajectories is very small and nearly indistinguishable after the transient phase, indicating that the controller ensures high tracking accuracy even under disturbances and actuator limitations.

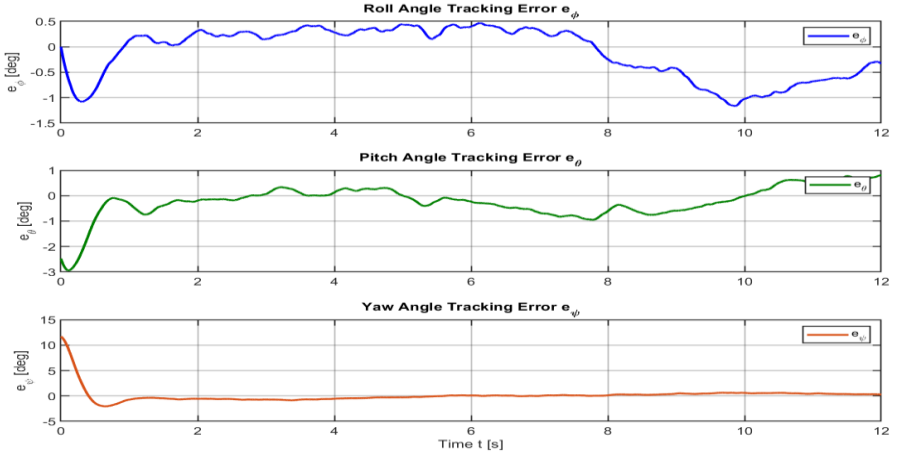

Figure 3. Euler Angle Tracking Errors

Figure 3 shows that the Euler–angle tracking errors of the IASMC controller rapidly converge to near zero after the initial transient phase. The roll and pitch errors decrease from approximately $-1°$ to $-3°$ to within $\pm 0.5°$ in only 1–1.5 seconds, demonstrating good stability despite measurement noise. The yaw axis exhibits a

larger initial error but converges the fastest and maintains very small oscillations around 0°. Overall, the controller yields small, stable, and low–oscillation angle errors, reflecting high trajectory–tracking performance and robustness against disturbances and uncertainties.

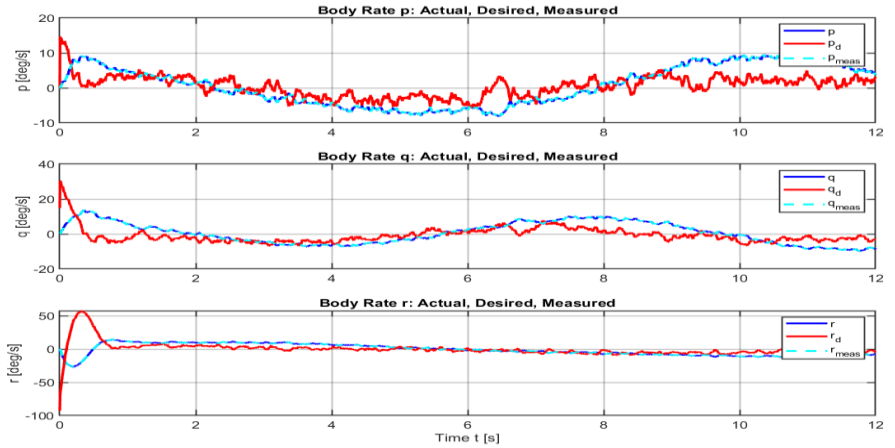

Figure 4. Tracking performance of body angular rates

Figure 4 presents the body–rate tracking performance for the three angular rates $p, q,$ and r. It can be observed that the actual angular rates follow the desired rates well after the initial transient phase, even under significant measurement noise. The yaw rate $r$stabilizes the fastest, whereas the p and $q$axes experience more noise influence but still maintain good tracking. This demonstrates that the adaptive controller adjusts the control gains appropriately to ensure angular–rate tracking under noise and actuator delays.

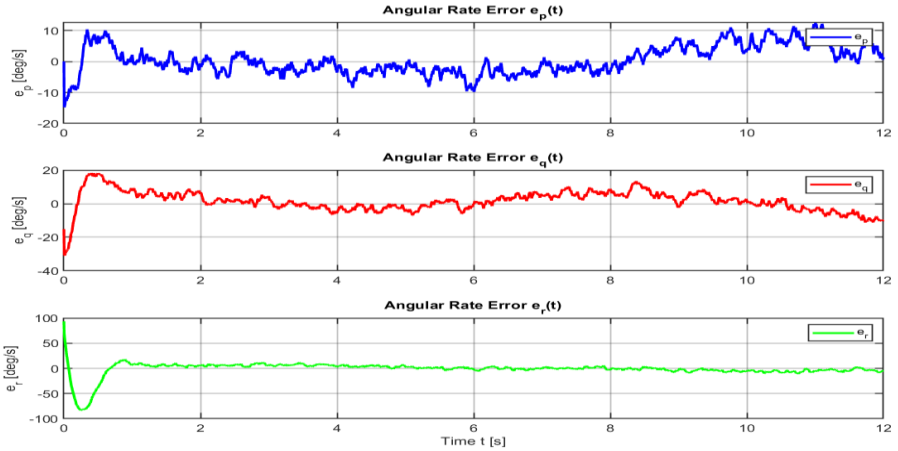

Figure 5. Angular rate tracking errors

Figure 5 illustrates the angular–rate tracking errors over time. All three axes exhibit large initial errors due to abrupt rate changes, especially the yaw rate error $e_r(t)$, which initially exceeds 100 deg/s. However, the errors quickly decrease and converge to near zero within about 1–1.5 seconds. Afterwards, the remaining small oscillations are primarily due to measurement noise. The yaw error shows the most stable behavior, while the roll $e_p(t)$and pitch $e_q(t)$errors oscillate slightly around zero but remain within acceptable bounds. These results demonstrate good angular–rate tracking performance and disturbance rejection capability.

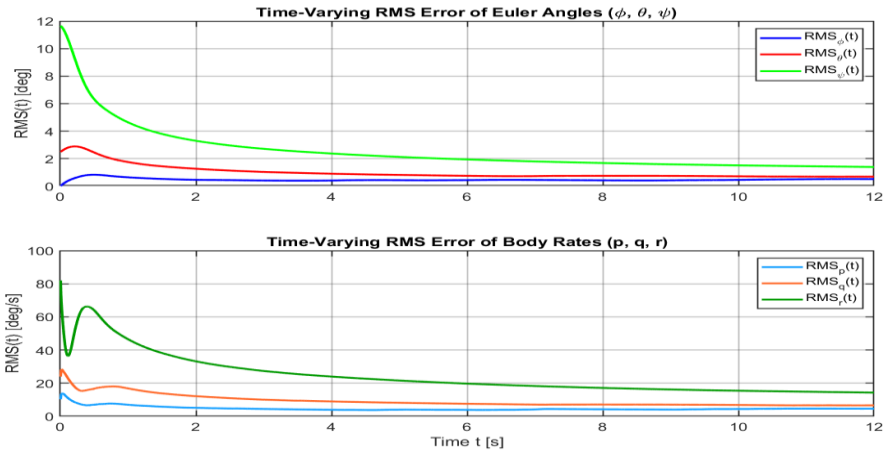

Figure 6. Time-varying RMS tracking error

Figure 6 shows that the RMS tracking errors of both Euler angles and angular rates decrease rapidly over time. Initially, RMS errors are relatively large due to abrupt trajectory changes, but they drop significantly and approach stable low values after about 2–3 seconds. The angle RMS values settle below 1°, while the angular–rate RMS values decrease to around 10–15°/s depending on the axis. This monotonic decreasing trend clearly indicates the convergence ability and long–term stability of the IASMC controller.

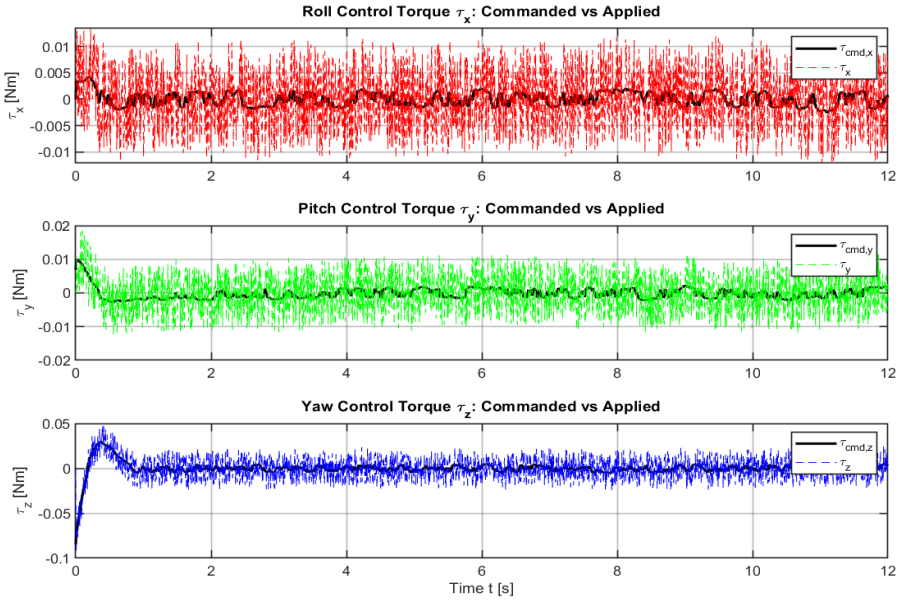

Figure 7. Commanded and applied control torques

Figure 7 shows that the control torques are continuously adjusted to satisfy angular–rate tracking requirements under disturbances and actuator limits. The applied torques (after delay) generally follow the commanded torques closely, indicating good compensation of the delay model. Although measurement noise and dynamic disturbances introduce small–amplitude fluctuations, the controlled torques remain within allowable bounds and do not lead to instability. The yaw axis produces the largest torque in the initial stage to compensate for large initial errors, then stabilizes to small amplitudes, reflecting the robustness of the controller.

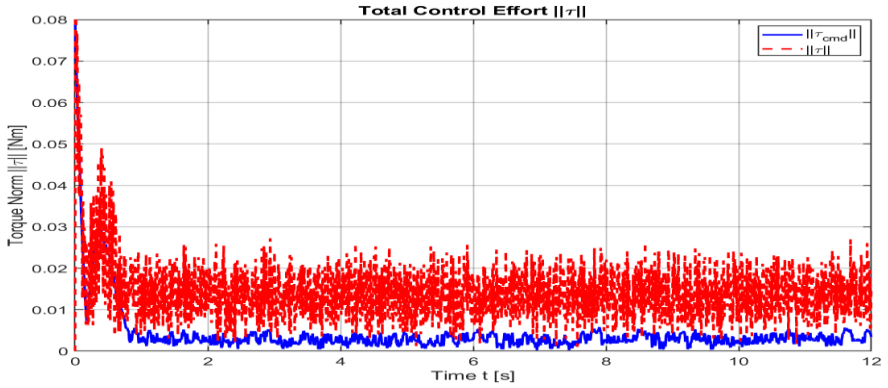

Figure 8. Total Control Effort Norm

Figure 8 displays the norm of the total control effort over time. Immediately after the transient phase, $\| \tau(t) \|$ rapidly decreases from a high value to a very low level (below 0.02 Nm) and remains stable throughout the process. This indicates that IASMC not only tracks well but also requires low control energy after convergence, significantly reducing vibrations and chattering. The small difference between commanded and actual torques further confirms the effectiveness of the delay–compensation mechanism.

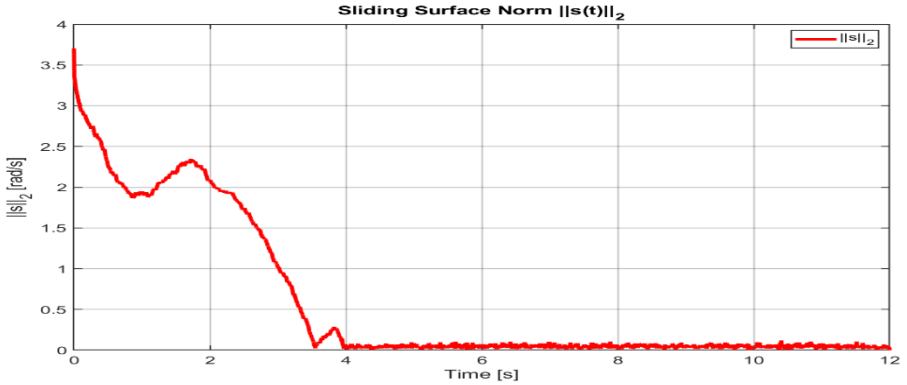

Figure 9. Norm of Sliding Surface

Figure 9 shows that the sliding–surface norm $\| s(t) \|_2$decreases sharply from about 3.6 to nearly zero within 3–4 seconds. After that, the norm remains very small and stable, indicating that the system truly adheres to the sliding manifold. This strongly confirms that the IASMC algorithm successfully brings the system into a stable sliding mode and maintains the sliding condition throughout the simulation, ensuring robustness and accuracy of the controller.

4. Conclusion

This paper has presented an IASMC for the quadrotor system based on the Newton–Euler dynamic model. The proposed method combines a two–loop control structure, in which the outer PD loop generates the desired angular rates, and the inner ASMC loop adjusts the control torques together with an adaptive law that updates the sliding gains over time. The adaptive mechanism is designed to automatically optimize the sliding gains in order to reduce chattering, improve tracking capability, and ensure stability under disturbances and model uncertainties.

Simulation results show that the IASMC achieves highly accurate tracking of Euler–angle and angular–rate trajectories, with fast error convergence, small oscillations, and control torques within allowable limits. The sliding surfaces and their norms quickly converge to near zero, confirming the establishment and maintenance of a stable sliding mode. The adaptive parameters $k_i(t)$ converge to equilibrium values without gain–explosion phenomena, demonstrating the robustness of the updating law. These results confirm the high effectiveness

and reliability of the IASMC for strongly nonlinear quadrotor systems under disturbance.

Integrating the adaptive mechanism directly into the sliding surface to adjust the sliding gains according to instantaneous error enables the controller to adapt well to state variations and disturbances while maintaining smoothness and significantly reducing chattering. Additionally, the comprehensive simulation with multiple realistic effects (sensor noise, disturbance torques, torque limits, and actuator delay) provides an in–depth and practical evaluation closely aligned with real operational conditions.

Declaration of Conflicting Interests

The authors declare no potential conflicts of interest with respect to the research, authorship and publication of this article.

Funding

The author received no financial support for the research, authorship and publication of this article.

References

[1] Shtessel, Y., Edwards, C., Fridman, L., & Levant, A. (2014). *Sliding mode control and observation*. Springer. https://doi.org/10.1007/978-0-8176-4893-0

[2] Zhang, Z., Li, Y., & Chen, D. (2024). Robust geometric control for quadrotor UAV with extended Kalman filter estimator. *Actuators, 13*(6), 205. https://doi.org/10.3390/act13060205

[3] Li, S., Wang, J., & Chen, W. (2024). Adaptive disturbance observer-based sliding mode control for quadrotor UAV. *Information Sciences, 667*, 120312. https://doi.org/10.1016/j.ins.2024.120312

[4] Hou, L., Zhang, J., Yu, Z., Wang, X., & Chin, C. S. (2025). Predefined-time sliding mode control for quadrotor UAV systems. *Scientific Reports, 15*, 39720. https://doi.org/10.1038/s41598-025-23330-2

[5] Huang, S., & Yang, Y. (2022). Adaptive neural-network-based fast terminal sliding mode control for quadrotor UAV. *Drones, 6*(8), 206. https://doi.org/10.3390/drones6080206

[6] Yogi, S. C., Tripathi, V. K., & Behera, L. (2021). Adaptive integral sliding mode control using neural networks for quadrotor UAV. *IEEE Transactions on Neural Networks and Learning Systems, 32*(12), 5595–5609. https://doi.org/10.1109/TNNLS.2020.3042031

[7] Rao, J., Li, B., Zhang, Z., & Chen, D. (2022). Position control of quadrotor UAV based on fuzzy neural network. *Energies, 15*(5), 1763. https://doi.org/10.3390/en15051763

[8] Ali, A. M., Hashim, H. A., & Jayasiri, A. (2025). Finite-time sliding mode control for quadrotor UAV systems. *arXiv preprint*. https://arxiv.org/abs/2507.20071

[9] Shevidi, A., & Hashim, H. A. (2024). Adaptive backstepping fast terminal sliding mode control for quadrotor UAVs. *arXiv preprint*. https://arxiv.org/abs/2407.01275

[10] Sun, C., Zhang, Y., & Wang, H. (2023). Robust adaptive sliding mode control for quadrotor UAV under disturbances. *Aerospace Science and Technology, 134*, 108139. https://doi.org/10.1016/j.ast.2023.108139

[11] Wang, X., Li, Z., & Chen, M. (2023). Neural-network-based adaptive control for quadrotor UAV systems. *IEEE Access, 11*, 45678–45689. https://doi.org/10.1109/ACCESS.2023.3274567